4

Bilayer TiO_2/SnO_2 ETL for efficient and stable perovskite solar cell

4.1 Broad Context

It is realized that an efficient electron transport layer (ETL) is essential to transport electrons and block holes, and to reduce the electrical shunting between transparent electrode/perovskite interface to enhance the performance and stability of perovskite solar cell (PSCs). TiO_2 is widely accepted ETL due to its wide bandgap, low cost and easy fabrication. However, TiO_2 tends to catalyse the degradation of the perovskite layer. On the other hand, SnO_2 shows better conductivity, mobility and stability with perovskite. Bilayer ETL is an effective way to transcend inherent limitations of single-layer ETL, which is very helpful in improving the performance as well stability of PSC [164].

4.2 Introduction

To achieve better and cheaper alternative energy, organic inorganic halide perovskite (OIHP) is rising as emerging photovoltaic (PV) technology to disrupt the dominance of silicon solar cell. PSCs have intriguing optoelectronic properties, including high absorption coefficient, long carrier diffusion length, and low trap state, which have experienced a series of breakthroughs and achieved a PCE of over 26% [33,165,166]. PSC device architecture consists of a transparent conductive oxide (TCO) based substrate (e.g. fluorine-doped tin oxide, FTO), an electron transport layer (ETL) usually consisting of an n-type metal oxide (TiO_2, SnO_2, ZnO), perovskite layer, a p-type organic or inorganic hole transport layer (HTL), and a metal top electrode (gold, silver) [27].

Titanium dioxide (TiO_2) is the most popular ETL material due to its chemical stability, non-toxicity, and good electrical properties [122]. TiO_2 is also a promising photocatalyst, which creates active trap sites under illumination that catalyses the degradation of the perovskite layer. At the same time, photo-generated electrons trapped at the deep sites combine with the photo-generated holes [132]. Moreover, pristine TiO_2 shows relatively lower electron mobility and requires high-temperature sintering (500°C) during synthesis. Tin oxide (SnO_2), on the other hand, has a deeper conduction band (CB) (better energy level matching with perovskite) and higher electron mobility (250 $cm^2V^{-1}s^{-1}$), which is about 100 times greater than TiO_2 [8]. In addition, SnO_2 exhibits excellent electrical properties, better transparency in the visible region, and lower photocatalytic activity [164,167]. However, SnO_2 exhibits an attenuated electron conductivity and carrier diffusion coefficient due to the defect-induced charge trapping-detrapping phenomenon [168]. Moreover, tin can take multiple valence states (+2 and +4), due to which SnO_2 layers are marred by the presence of point defects, such as oxygen vacancies, which act as charge recombination centres [169]. To address these issues, introducing a bilayer ETLs composed of different binary metal oxides (TiO_2-SnO_2) to improve the electron extraction and to enhance stability of perovskite without compromising device performance could be a viable approach [164,170].

The interfacial morphology between ETL and perovskite film is important for efficient charge transfer and for improved stability of PSC. Wettability and roughness of the substrate layer can affect the microstructure of the as deposited films. In PSCs achieving a compact microstructure of perovskite film is important as defects and pores can absorb moisture and degrade the films faster. There is very few study on the effect of ETL layer on the microstructure and stability of perovskite films.

Herein, we have investigated the effect of wettability and roughness on the microstructure and the degradation of $FAMAPbI_3$ perovskite layer deposited over TiO_2, SnO_2 and TiO_2/SnO_2 bilayers. A complete cell based on different ETLs is fabricated to explore the role ETLs on the overall performance of PSC.

4.3 Role of ETL in perovskite solar cell

ETLs in PSCs, ease the movement and decrease the potential energy barrier of electron transfer to the cathode and blocks the hole after the charge separation when the light is absorbed by the sensitizer material [171]. It also attributes in better energy alignment between the absorber layer and the electrode material. ETLs should meet some of the requirements in device architecture such as (1) high transparency to allow efficient light harvesting, (2) well-matched energy alignment to trigger electron transfer while blocking holes, and (3) high electron mobility to minimize the charge accumulation [172,173].

4.4 Experimental

TiO_2, SnO_2 and TiO_2-SnO_2 bilayer films were deposited on FTO substrates by spray pyrolysis method, mentioned in Chapter 2 [122]. In brief, SnO_2 film was prepared by spraying the precursor solution prepared by dissolving 189 mg $SnCl_2$ (99.99%, Sigma Aldrich) in 10 ml methanol at 400°C followed by annealing at 450°C for 30 minutes. The perovskite solution ($FA_{0.5}MA_{0.5}PbI_3$) prepared by mixing 86 mg of formamidinium iodide (FAI, Great cell solar), 79 mg of methyl ammonium iodide (MAI, Great cell solar), and 461 mg lead iodide (PbI_2, Sigma Aldrich, 99%) in mixture of DMSO and DMF (1:4) was spin coated by three-step spin coating process: 500 rpm for 10 s, 1500 rpm for 15 s, and 3000 rpm for 30 s, and during the last step, 100 µl CB (Sigma Aldrich 99.98%) were dripped as an antisolvent, then annealed at 100°C for 10 minutes on hotplate [68]. 72.3 mg of Spiro-OMeTAD, 29 µL of TBP and 18 µL of Li-TFSI (520 mg Li-TFSI in 1 mL acetonitrile, 99.8%, Sigma-Aldrich) dissolved in 1mL of

CB (99.9%, Sigma Aldrich). The solution was spin coated at 4000 r.p.m for 30 seconds. Finally, 90-100 nm gold (Au) was thermally evaporated at 10^{-5} mbar.

4.5 Result and Discussion

Figure 4.1a-c shows the XRD patterns of TiO_2, SnO_2 and TiO_2-SnO_2 ETLs. The well-defined diffraction peaks in **Figure 4.1a and b** confirms the phase pure TiO_2 and SnO_2 films, while **Figure 4.1c** shows diffraction peaks corresponding to both SnO_2 and TiO_2. Even though the Sn has a higher scattering factor and SnO_2 has higher density (6.93 g/cc) when compared to TiO_2 (density 4.2 g/cc), the diffraction peaks intensity of TiO_2 was greater indicating that the SnO_2 layer was relatively thinner. A relatively higher background is observed in all the cases due to the glass substrate. In case of SnO_2 and bilayer the diffraction peaks were less intense mainly due to the lower degree of crystallinity of SnO_2. **Figure 4.1d-f** depicts SEM images of TiO_2, SnO_2 and TiO_2-SnO_2. All the films were dense and covered the substrate uniformly, and there was absence of pinholes and defects which is the basic criterion for achieving good perovskite film when coated above the ETL substrate. The thickness of the films was ≈ 60 nm, ≈ 77 nm and ≈ 85 nm for the TiO_2, SnO_2 and TiO_2-SnO_2 bilayer films, respectively.

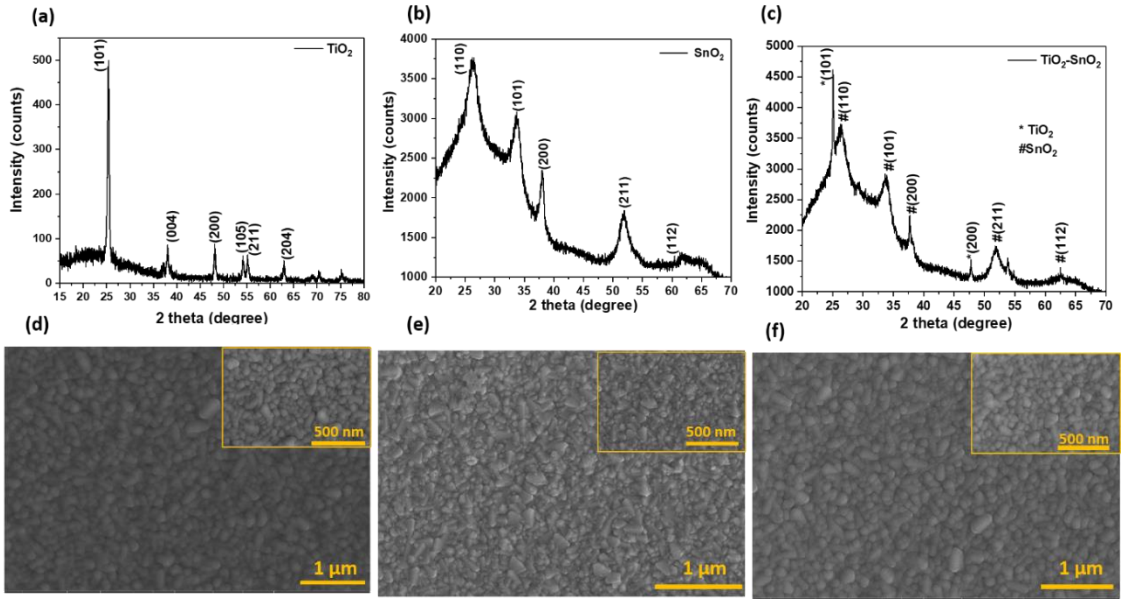

Figure 4.1. XRD plot of a) TiO_2, b) SnO_2 and c) SnO_2-TiO_2, SEM images of d) TiO_2, e) SnO_2 f) TiO_2-SnO_2.

The AFM was carried out in a NT MDT (Moscow, Russia) machine using nanocrystal silicon tips in tapping mode to look at the surface topography, roughness and the grain size of the ETL films **(Figure 4.2 a-c).** It has been observed that RMS value in TiO_2 (18.097 nm) and SnO_2 (21.24 nm) were higher than bilayer ETL (14.06 nm). At the same time, much smaller grains were observed in both TiO_2 (121 nm) and SnO_2 (166 nm) than the bilayer ETL (218 nm) as illustrated in SEM images **(Figure 4.1 d-f).** Surface energy plays an important role in deciding the coverage adhesion during film deposition. The contact angle measurements were made to get an idea of the relative wettability of perovskite solution on the ETL layer (**Figure 4.3 a, c, e**). The contact angle of both TiO_2 and bilayer films was lower (~37° and 39°, respectively), while SnO_2 has the highest contact angle of 44°. This indicates that the perovskite solution would wet the TiO_2 surface more easily than the other two cases. This indicates that the perovskite solution will spread more uniformly on TiO_2 than SnO_2.

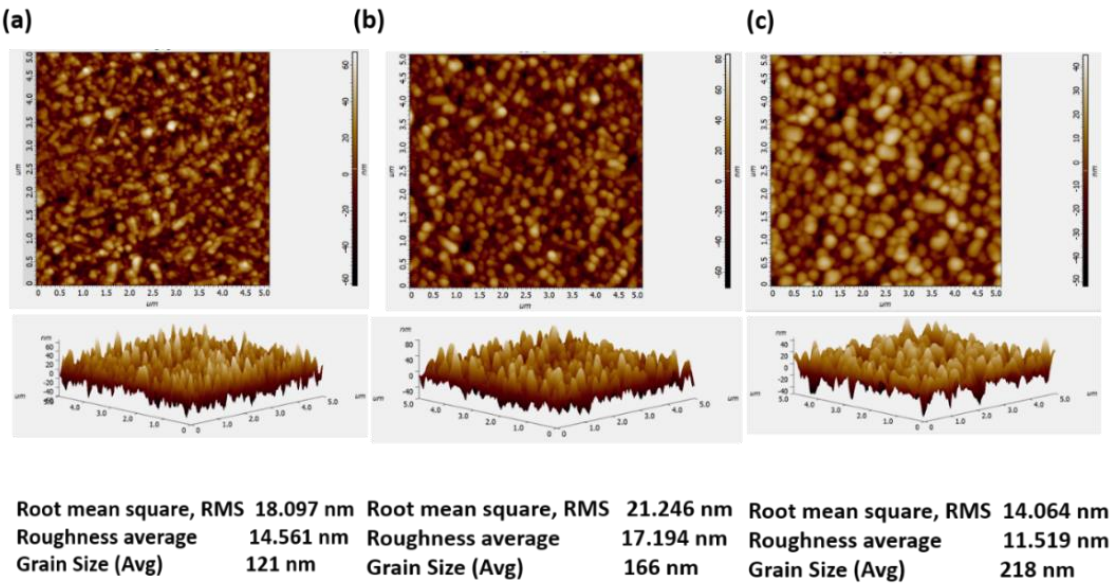

Figure 4.2. Surface topography images and the roughness of a) TiO_2, b) SnO_2 and c) TiO_2-SnO_2 respectively.

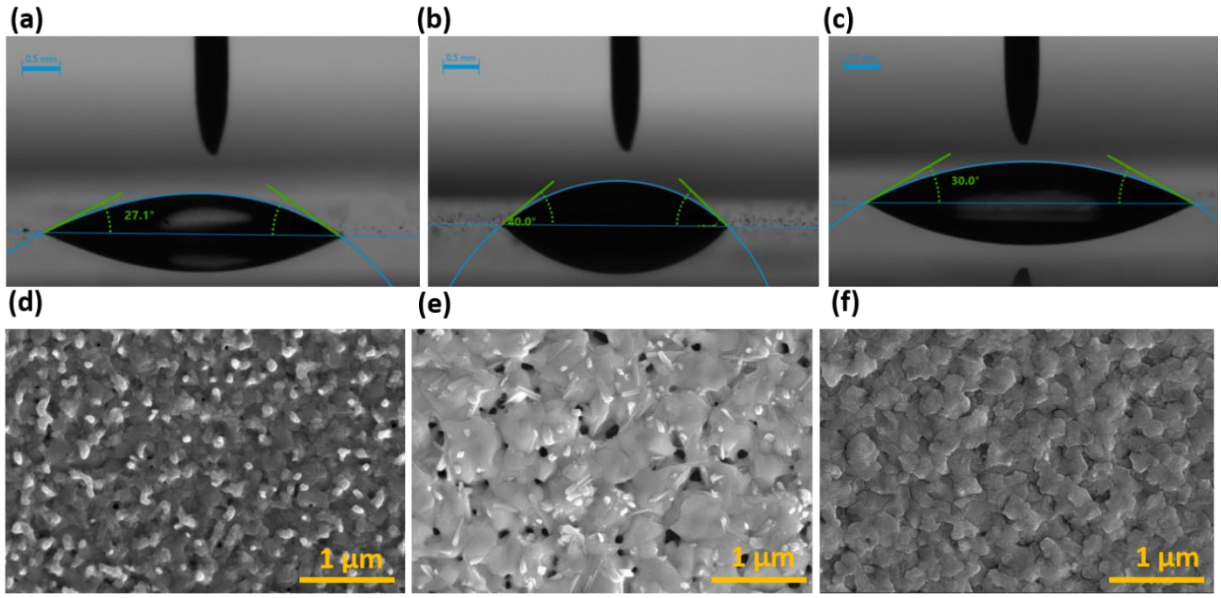

Figure 4.3 Contact angle measurement of perovskite solution and SEM images of $FAMAPbI_3$ on a, d) TiO_2, b, e) SnO_2 and c, f) TiO_2-SnO_2 respectively.

The effect of wettability on the film morphology is verified by SEM images of perovskite ($FAMAPbI_3$) deposited on different ETLs (**Figure 4.3 d, e, f**). Perovskite forms a smooth

surface when deposited on TiO_2 (**Figure 4.3 d**), while the films are disrupted and have gaps when deposited on SnO_2, **(Figure 4.3 e)** which could lead to direct contact between FTO and perovskite causing serious recombination. Whereas the film coated on bilayer TiO_2-SnO_2 is well-packed without any visible pinholes **(Figure 4.3 f).** The more compact and uniform film with much lower roughness **(Figure 4.2)** over the bilayer is due to the greater wettability of the TiO_2-SnO_2 confirmed by the lower contact angle. A lower contact angle, i.e. greater wettability favours a faster rate of nucleation and growth and continuity of the film. In contrast, a lower wettability hinders the nucleation event and makes it more prone to discontinuities [174]. Moreover, a smoother surface would lead to bigger grain sizes, while a rough surface can provide more nucleation sites for the formation of crystalline structures and smaller grains [175].

XRD pattern of $FA_{0.5}MA_{0.5}PbI_3$ films were recorded at regular time intervals, for up to 60 days, to monitor the stability of the film. All the major peaks in the freshly prepared samples could be indexed to the $FAMAPbI_3$ tetragonal phase [11] **(Figure 4.4 a-c).** An additional peak (at $2\theta=11.31°$) corresponding to the δ-$FAMAPbI_3$ is also present. The peak corresponding to the δ-phase is much more intense in the film deposited on TiO_2 than on SnO_2 and TiO_2-SnO_2 bilayer, suggesting negligible phase separation in the later two cases. After 20 days, peak corresponding to PbI_2 (at $2\theta=12.53°$) appears in the case of TiO_2 indicating the beginning of decomposition of the perovskite phase, whereas the other two films remained intact **(Figure 4.4 a-c).** After 45 days, the PbI_2 peak becomes more intense and the colour of the perovskite film on TiO_2 becomes brownish, while no such signs of decomposition are observed in films deposited on SnO_2 and TiO_2-SnO_2. After 60 days, perovskite films turned completely yellow indicating the complete decomposition of the film coated on the TiO_2 layer. On the other hand, in the case of SnO_2 the PbI_2 peak was absent even after 60 days whereas, a comparatively much less intense PbI_2 peak is seen in films deposited on TiO_2-SnO_2 **(Figure 4.4c).** This observation

indicates that the $FAMAPbI_3$ films deposited on TiO_2-SnO_2 bilayer was more stable while the films deposited on the TiO_2 was least stable. Similarly, **Figure 4.4d** depicts the summary of observed delta and alpha peak in perovskite layer, the ratio of intensity of delta (I_δ) to intensity of alpha ($I\alpha$) is plotted against the time (days), it is shown that in case of TiO_2 alone the ratio is exponentially increased while in case of SnO_2 and TiO_2-SnO_2 ETL the graphs changes linearly demonstrating negligible change throughout in SnO_2 and bilayer TiO_2-SnO_2 which exhibits the least degradation of perovskite film and remain stable till 60 days. This shows the importance of ETL layer and its wettability, roughness and in deciding the microstructure, properties and stability of the perovskite film.

The electrical properties of different ETLs were probed by Hall effect measurement. It is shown that bilayer ETL has better conductivity (10.98 $\Omega^{-1}cm^{-1}$) and less resistivity (0.091 Ω-cm) as compared to the TiO_2 (0.0301 $\Omega^{-1}cm^{-1}$), (331.2 Ω-cm) and SnO_2 (2.7578 $\Omega^{-1}cm^{-1}$), (0.36267 Ω-cm) alone, which is prerequisite for an efficient ETLs. The thickness for the TiO_2, SnO_2 and TiO_2-SnO_2 are ≈ 60 nm, ≈ 77 nm and ≈ 85nm respectively.

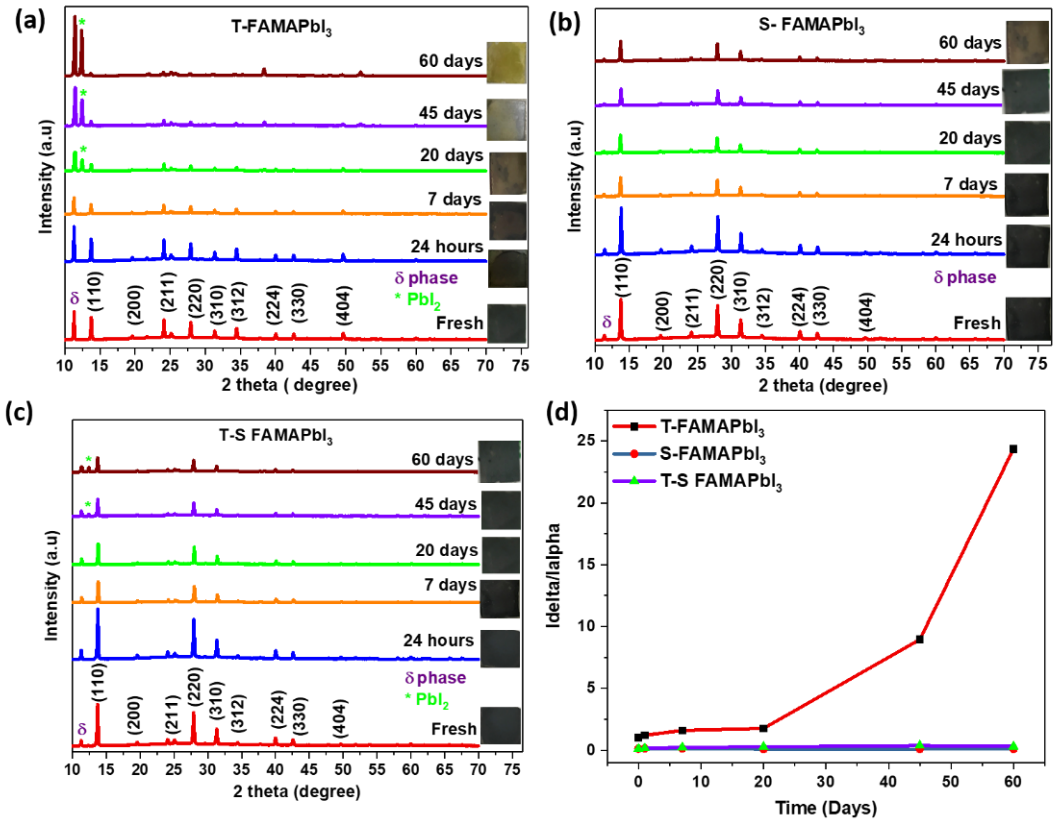

Figure 4.4. XRD plots showing the stability of $FAMAPbI_3$ film with time on a) TiO_2 (T), b) SnO_2 (S) and c) TiO_2-SnO_2 (T-S) and d) degradation of $FAMAPbI_3$ film with days on different ETL.

UV Vis of TiO_2, SnO_2 and bilayer ETL were done to check the optical properties of the ETLs, the absorbance, bandgap and their respective transmittance of all the ETLs are shown in **Figure 4.5a-f.** It is believed that ETL should have wide band gap and higher transparency which could transmit most of the light to absorber layer. The band gap (Tauc plot) and transparency of TiO_2, SnO_2 and bilayer TiO_2-SnO_2 are 3.53 eV, 3.9 eV, 3.63 eV and 90%, 95% and 85%, respectively, in visible region which is very much required for efficient ETL [169,170].

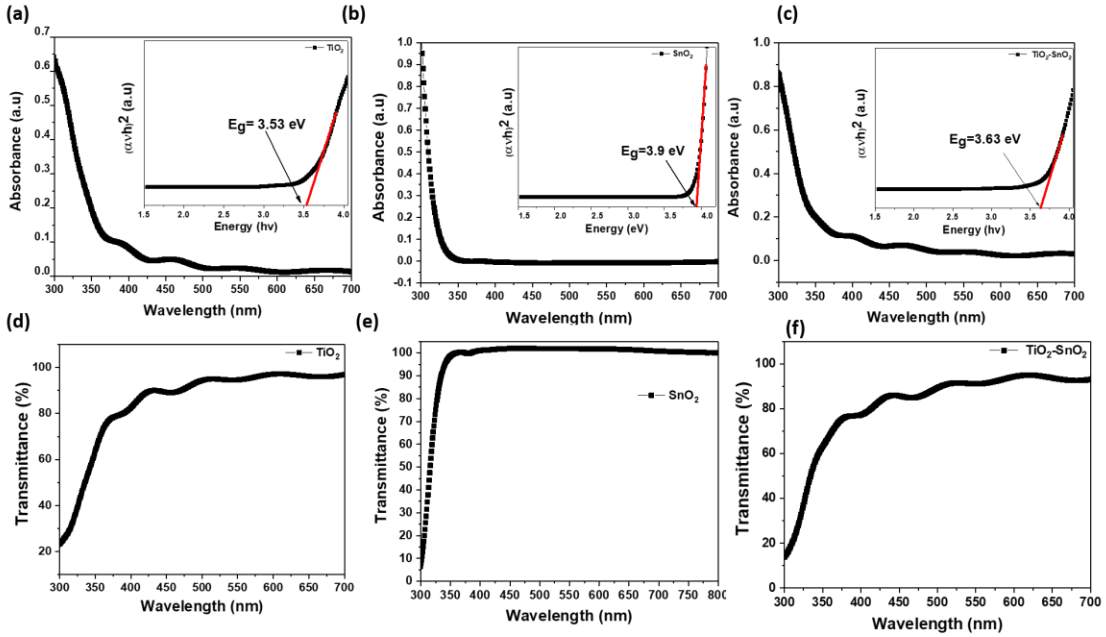

Figure 4.5. Absorbance, Tauc plot (inset) and transmittance of a, d) TiO_2, b, e) SnO_2 and c, f) TiO_2-SnO_2 respectively.

The absorbance and the bandgap (1.45 eV, calculated from the Tauc plot) of freshly prepared $FAMAPbI_3$ films deposited on different ETL layers are identical **(Figure 4.6 a-c)** [12]. The PL peak between 770 and 780 nm **(Figure 4.6 d)** matches closely with the band gap of $FAMAPbI_3$, indicating the band-to-band transition. Bilayer TiO_2-SnO_2 exhibits a comparatively stronger quenching effect, which suggests enhanced charge extraction at the ETL/perovskite interface [176].

Finally, to look at the effectiveness of the deposited ETL layers, solar cells with a layer sequence FTO/ETLs/$FAMAPbI_3$/Spiro-OMeTAD/Au was fabricated. The major performance parameters were recorded using different ETLs. **Figure 5e** displays the J–V curves of PSCs fabricated on different ETLs. The PSC on TiO_2 ETL had a PCE of 10.27% with a V_{oc} of 0.8V, a short-circuit current density (J_{sc}) of 22 $mAcm^{-2}$, and a fill factor (FF) of 58%. On the other hand, SnO_2-ETL based PSC has a PCE of 10% with V_{oc} of 0.83 V, J_{sc} of 26 $mAcm^{-2}$ and FF of 45%. It can be seen in case of TiO_2 alone J_{sc} is much less than SnO_2 due to the lower

conductivity of TiO_2 as also confirmed by the Hall measurement. The reason for the poor FF in case of SnO_2 is poor morphology with numerous pinholes and cracks in perovskite film deposited on SnO_2. The modified bilayer TiO_2-SnO_2 device achieves a champion PCE of 13% with V_{oc} of 0.82 V, J_{sc} of 26 $mAcm^{-2}$ and with highest FF of 60% (**Figure 5f**). The increase in PCE is attributed to the improved FF. The FF of the PSC fabricated on the bilayer film is mainly because of uniformity of the film microstructure (due to better wetting of precursors) and the greater electronic conductivity of SnO_2 and graded band alignment [177]. The better morphology of perovskite on bilayer ETL is attributed to less rough surface, and lower contact angle, i.e. greater wettability quickens the rate of nucleation and growth and continuity of the film, while in case of TiO_2 and SnO_2 a lower wettability hinders the nucleation event and makes it more prone to discontinuities. Moreover, a smoother surface in case of bilayer (RMS value 14.06nm) contributes in bigger grain sizes, compactness and uniformity while rough surface in other two (TiO_2 and SnO_2) showed smaller grains and some pinholes and non-uniformity in morphology. Besides this, the bilayer ETL has improved the optoelectronic properties, an enhanced electrical conductivity and suitable wider bandgap (E_g=3.63 eV) allows the more photons to falls on the perovskite layer resulting in large number of photo generated electrons which is responsible for achieving better J_{sc} of 26 $mAcm^{-2}$. This shows that how efficiently the bilayer TiO_2-SnO_2 helps in improving the morphological, optical, electrical properties of ETLs and enhancing the stability the overall performance of PSC.

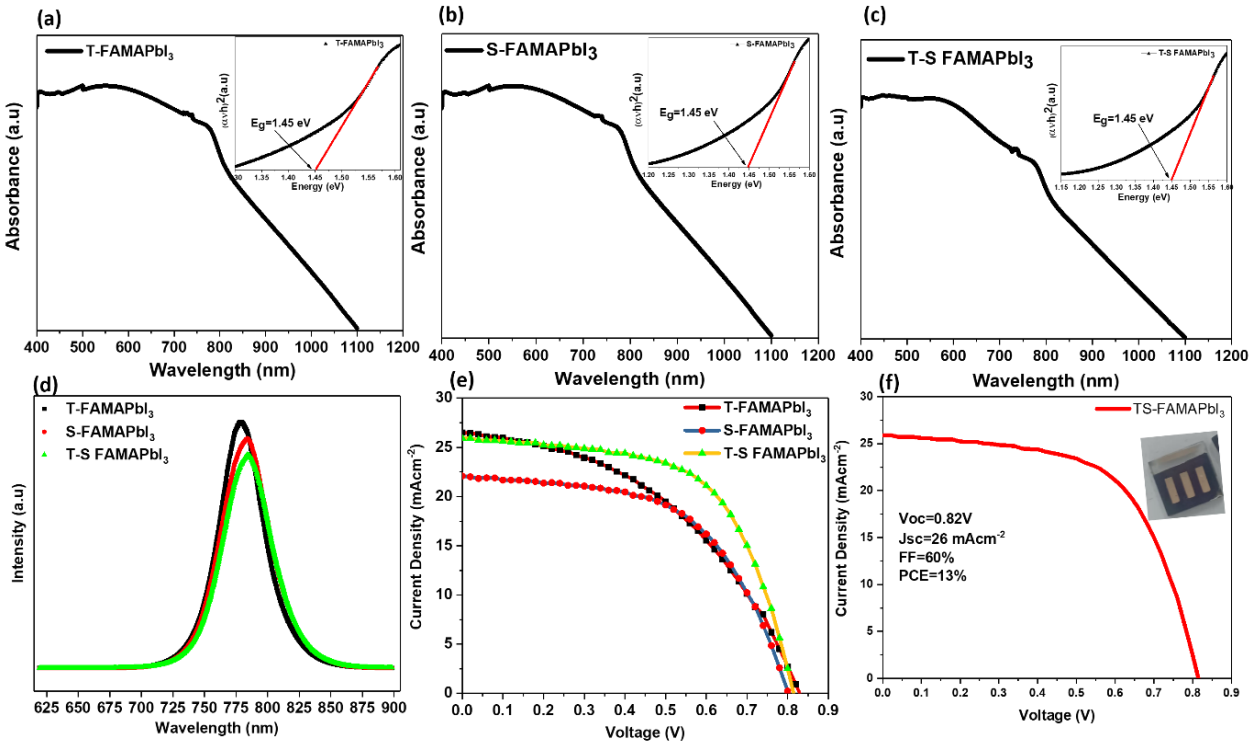

Figure 4.6. Absorbance and Tauc plot (inset) of perovskite ($FAMAPbI_3$) film on a) TiO_2, b) SnO_2 and c) SnO_2-TiO_2. d) PL measurement of perovskite film deposited on TiO_2 (T), SnO_2 (S) and TiO_2/SnO_2 bilayer (T-S). e) J-V of PSC fabricated on different ETLs f) J-V curve of the champion cell fabricated on bilayer TiO_2-SnO_2 ETL. Inset showing the photograph of the cell.

4.6 Conclusion

The basic criterion for ETL is explored considering the three different ETLs namely TiO_2, SnO_2 and bilayer TiO_2-SnO_2. The XRD confirms the synthesis of TiO_2, SnO_2 and bilayer ETL while SEM and AFM shows the morphology and surface topography, which confirms compact and dense film with bigger grain size. The higher wettability and lower roughness of ETL substrates assisted in achieving better compactness and uniformity of film morphology. The absence of defects and discontinuities improved the stability of perovskite films on bilayer ETL and have shown stability up to 60 days in ambient air (RH = 70%). At the same time, the PL peaks show greater quenching and more efficient electron extraction at the bilayer-ETL/perovskite interface.

Moreover, the bilayer TiO_2-SnO_2 device achieves a champion PCE of 13% with V_{oc} of 0.82 V, J_{sc} of 26 $mAcm^{-2}$ and with highest FF of 60%. This shows the efficacy of bilayer TiO_2-SnO_2 in improving the morphological, optical, electrical properties of ETLs and enhancing the stability the overall performance of PSC.